Nitrogen-doped Carbons Derived from Poly(ionic liquid)s of Various Backbones and Cations

Rui Sun, [1] *Kelly M. Meek,* [2] *Hoi Chun Ho,* [3] *Yossef A. Elabd* [1]*

[1] Department of Chemical Engineering, Texas A&M University, College Station, TX 77843, United States

[2] National Renewable Energy Laboratory, 15013 Denver W Parkway, Golden, CO 80401, United States

[3] The Bredesen Center for Interdisciplinary Research and Graduate Education, The University of Tennessee, Knoxville, TN 37996, United States

* To whom correspondence should be addressed; E-mail: elabd@tamu.edu

ABSTRACT: In this study, poly(ionic liquid)s (PILs) with various backbone/cation pairings (backbones: ethyl methacrylate, styrene; covalently attached cations: butylimidazolium, trimethylammonium, butylpyrrolidinium) were successfully synthesized as carbon precursors. Pyrolysis of PILs produced carbons with sheet-like structures with a metallic luster in contrast to the powder form of carbons produced from polyacrylonitrile (PAN). Results also show that cation type has a significant impact on surface area, graphitic content, graphitic nitrogen content, nitrogen retention, carbon yield, and surface chemistry of the PIL-derived carbons. The design of nitrogen-doped carbons based on a diverse set of PILs with various cation and polymer backbone

chemistries may be an effective strategy to optimize carbon properties for subsequent application in energy storage devices.

Keywords: ionic liquid, polymer, carbon, nitrogen, graphitic, capacitor, battery

INTRODUCTION

Carbon has been extensively investigated due to its outstanding advantages and properties, including accessibility, low cost, non-toxicity, high chemical stability, high strength-to-weight ratio, electrical conductivity, and electrocatalytic activity.[1-3] Therefore, the development of new carbon materials with exquisite control over surface chemistry, surface area, pore size, and conductivity is of significant interest for numerous applications, including energy storage (*e.g.*, batteries, capacitors). Numerous types of carbon with different morphologies and properties have been investigated, where a variety of factors have been shown to impact the structure and properties of carbon materials, including pore size and pore size distribution,[1, 4-7] surface chemistry,[8] and incorporation of heteroatoms.[9] Specifically, heteroatoms (N, S, P, F) introduced into carbon frameworks may successfully modify the chemical structure of carbon materials and result in electrode materials with enhanced electronic conductivity,[7, 10] capacitance,[11-15] and charge-discharge cyclability.[16] Among various heteroatom-doped carbons, nitrogen-doped carbon has been widely investigated due to its high electrical conductivity[7, 10] and catalytic activity.[17, 18] The nitrogen atoms in the carbon matrix can improve the charge mobility by changing the electron donor-acceptor characteristics and can give rise to pseudocapacitance *via* fast and reversible Faradic redox reactions with ions in electrolytes.[16, 19-21] The conductivity and catalytic activity of carbon materials can also be improved by creating conjugation between the p electrons of nitrogen

and the π-system of the carbon lattice,[22] leading to potential applications as electrode materials for energy storage systems,[23] metal-free catalysts for oxygen reduction reaction (ORR),[17, 18] and absorbents for CO_2 capture.[15, 24]

There are typically two strategies to prepare nitrogen-doped carbons: (1) post-treatment of carbon with nitrogen containing reagents and (2) carbonization of nitrogen rich precursors *via* pyrolysis.[25] Compared to the post-treatment strategy, carbonization of nitrogen rich precursors provides a more homogeneous distribution of the nitrogen atoms in bulk and may result in products with higher nitrogen content. Polyacrylonitrile (PAN) is one of the most widely studied polymer precursors for carbon production.[26-29] For example, Park *et al.*[26] electrospun PAN nanofibers and successfully carbonized the fibers at 1000 °C to yield carbon nanofibers as platinum catalyst supports for polymer electrolyte membrane fuel cells. Enhanced fuel cell performance was observed due to the partially aligned morphology and improved electrical conductivity. Zhong *et al.*[27] achieved nanoporous carbon structures by the pyrolysis of a poly(n-butyl acrylate) (PBA)-*b*-PAN block copolymer with well-defined, phase-separated morphology. The PBA block was selectively removed during carbonization at 700 °C, leaving behind a porous structure with high surface area. High capacitance per unit surface area was achieved due to the incorporation of nitrogen atoms. However, a lack of control over the resulting carbon morphology limits the use of the PAN homopolymers as a carbon precursor. Approaches, such as electrospinning and block copolymer precursor templating, are typically required for achieving a desired porous structure and high surface area. As a result, future investigations are of interest to develop novel nitrogen-doped carbon precursors with diverse chemical compositions that will subsequently improve properties, such as nitrogen content and surface area.

Ionic liquids (ILs), which are salts that contain an organic cation and an organic or inorganic anion and typically have a melting point below 100 °C, have recently been explored as carbon precursors.[30] ILs have been extensively investigated and applied in various fields (*e.g.,* catalysis,[31] polymer synthesis,[32] electrochemistry[33]) due their remarkable physicochemical properties, including negligible volatility, nonflammability, molecular tunability, high ionic conductivity, outstanding chemical and thermal stability, and wide electrochemical window. Recent studies have successfully demonstrated the ability to produce carbon from ILs, which results in carbon with various surface chemistries depending on the chemistry of the IL.[22, 34-40] The advantages of using ILs as nitrogen-doped carbon precursors include: (1) higher yield of the resulting nitrogen-doped carbon attributed to the negligible volatility and high thermal stability of ILs as a result of their charged nature[40] and (2) tunable morphology and heteroatom content of the resulting nitrogen-doped carbons due to the broad chemical diversity from numerous choices of cations and anions. Paraknowitsch *et al.*[34] discovered that mesoporous nitrogen-doped carbon can be produced by heating ILs in a mesoporous silica template at 1000 °C, where a high mass yield was achieved with the advantage of negligible volatility to minimize the loss of IL precursor during heating before decomposition. However, due to the mobility of the liquid state, the main drawback of using ILs as nitrogen-doped carbon precursors is the complication of achieving desired carbon structures in the absence of suitable templates.[25]

Polymerized ionic liquids or poly(ionic liquids) (PILs) are a distinct type of polymer that possesses the IL moiety in each repeat unit. Different from ILs, where both cations and anions are mobile, the cations of PILs are constrained (covalently attached) to each repeat unit of the polymer chain.[30] As solid alternatives of ILs, PILs are easier to be molded into desired shapes and applied as polymer precursors to achieve nitrogen-doped carbon with various morphologies. Higher

carbon yields can be obtained compared to IL-derived nitrogen-doped carbon as a result of the additional backbone immobilization. Recently, several PILs have been investigated as nitrogen-doped carbon precursors.[24, 25, 39-46] Yuan *et al.*[39] successfully demonstrated that a comparably well-developed mesoporous carbon structure with high electric conductivity could be achieved by the pyrolysis of ILs and PILs in the presence of iron salts, followed by the removal of the iron salt byproducts *via* acid etching. They found that 900 °C is a threshold temperature to develop high surface area carbons with low resistance. Zhao *et al.*[43] reported on the formation of micro/mesoporous nitrogen-doped carbons without using templates or activation agents by the pyrolysis of a PIL (poly[3-cyanomethyl-1-vinylimidazolium bis(trifluoromethanesulfonyl)imide (TFSI)]) at intermediate temperatures (500 to 800 °C). The bulky anion (*i.e.,* TFSI) serves as a molecular template and facilitates the formation of a porous structure during the formation of the carbon. However, to date, studies on PIL-derived nitrogen-doped carbons have almost exclusively explored vinyl polymers with covalently attached unsaturated nitrogen heterocyclic cations (*e.g.,* imidazolium, pyridinium, *etc.*). Few studies have explored the relationship between the possible diverse PIL chemistries (*i.e.,* polymer backbone, saturated heterocyclic cations) and the resulting PIL-derived carbon properties.

In this study, four PILs with various backbone/cation pairings (backbones: ethyl methacrylate, styrene; covalently attached cations: butylpyrrolidinium, butylimidazolium, trimethylammonium) were successfully synthesized as carbon precursors (Scheme 1). Owing to the combination of various thermal decomposition reactions in the carbonization process, the resulting carbons may obtain different carbon yield, composition, porosity and graphitic structure.[22] The carbon structure, degree of graphitization, surface area and porous structure, and surface chemistry of the PIL-derived carbons were characterized and compared to PAN-derived carbons. These results establish

a fundamental investigation into the relationship between various chemistries of PILs and PIL-derived carbon properties.

Scheme 1. Chemical structures of PILs with various backbone/cation pairings.

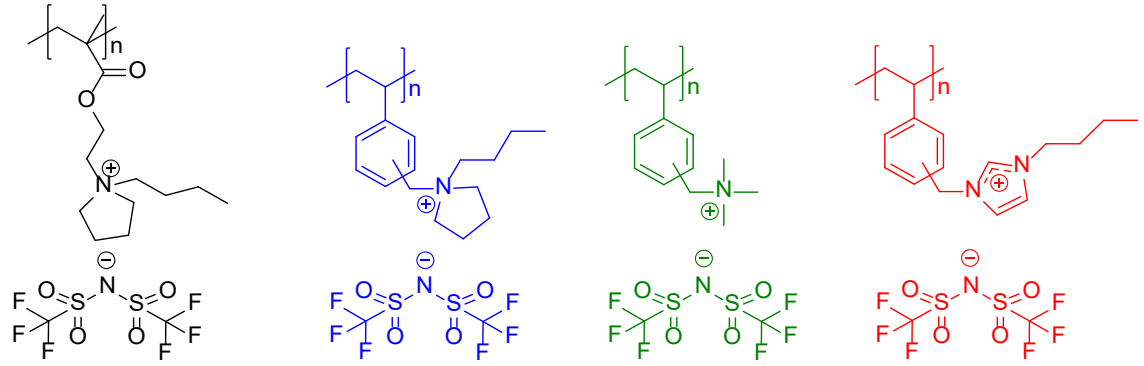

EXPERIMENTAL

Materials. Methacryloyl chloride (97%, contains ~200 ppm monomethyl ether hydroquinone as stabilizer), 2-bromoethanol (95%), triethylamine (≥99%), dichloromethane (anhydrous, ≥99.8%, contains 40-150 ppm amylene as stabilizer), magnesium sulfate (anhydrous, ReagentPlus®, ≥99.5%), sodium bicarbonate (powder, BioReagent, for molecular biology, suitable for cell culture, suitable for insect cell culture), 4-cyano-4-(phenylcarbonothioylthio)pentanoic acid (chain transfer agent (CTA), >97%, HPLC), tetrahydrofuran (THF, anhydrous, ≥99.9%), methanol (anhydrous, 99.8%), poly(vinylbenzyl chloride) (60/40 mixture of 3- and 4-isomers, M_n ~55.0 kg mol^{-1}, M_w ~100 kg mol^{-1} by GPC/MALLS), N, N-dimethylformamide (DMF, ACS Reagent, ≥99.8%), 1-butylimidazole (98%), trimethylamine solution (45 wt% in H_2O), 1-butylpyrrolidine (98%), hexane (anhydrous, 95%), diethyl ether (anhydrous, ≥99.7%, contains 1 ppm BHT inhibitor), acetone (ACS reagent, ≥99.5%), dimethyl sulfoxide-d_6 (DMSO-d_6, 99.9 atom % D, contains 0.03% v/v TMS), acetonitrile-d_3 (≥99.8 atom % D), deuterium oxide (D_2O, 99.98 atom% D), and

polyacrylonitrile (PAN, average M_w = 150 kg mol^{-1}) were purchased from Sigma-Aldrich and used as received without further purification. Bis(trifluoromethane)sulfonimide lithium salt (LiTFSI) (98+%) was purchased from Alfa Aesar and used as received without further purification. Azobis(isobutyronitrile) (AIBN, 98%, Sigma-Aldrich) was purified by recrystallization twice from methanol. Deionized (DI) water with resistivity *ca.* 16 MΩ cm was used as appropriate.

Synthesis of Poly(BrEMA). The synthesis of the monomer 2-bromoethyl methacrylate (BrEMA) was performed following literature procedure.[47] Reversible addition-fragmentation chain transfer (RAFT) polymerization was utilized to synthesize the non-ionic homopolymer precursor poly(BrEMA), as shown in step 1 of Scheme 2(a). An example reaction: 15.0120 g of BrEMA (77.7 mmol), 72.7 mg of CTA (0.260 mmol), 4.4 mg of AIBN (0.0268 mmol), and 2.9985 g THF were combined in a 250 mL single-neck Schlenk flask under continuous mixing. The reactor was subjected to three freeze-pump-thaw degassing cycles. Followed by sealing the reactor and thawing in water bath, the reaction was carried out under N_2 at 70 °C for 5 h. The resulting polymer was precipitated in methanol, filtered, and then dried under vacuum in an oven at room temperature for 24 h. Yield: 6.04 g of pink solid particles (40%). ^{1}H NMR (Mercury 500 MHz, $CDCl_3$, 23 °C) δ (ppm): 4.47-4.19 (s, 2H, O-C*H*$_2$-CH$_2$-Br), 3.66-3.47 (s, 2H, O-CH$_2$-C*H*$_2$-Br), 2.12-1.84 (d, 3H, CH$_2$-C(C*H*$_3$)), 1.12 (s, 1H, *H*CH-C(CH$_3$)), 0.98 (s, 1H, HC*H*-C(CH$_3$)) (NMR, Figure 1). GPC (THF, 40 °C): M_n = 19.02 kg mol^{-1}, M_w/M_n = 1.82 (against PS standards).

Synthesis of Poly(MEBPyr-TFSI). The synthesis procedure of poly(MEBPyr-TFSI) [MEBPyr-TFSI = 1-[(2-methacryloyloxy) ethyl]-1-butylpyrrolidinium bis(trifluoromethane) sulfonimide] is shown in step 2A of Scheme 2(a). An example reaction: 1.0004 g (5.18 mmol) of poly(BrEMA)

was dissolved in 12 mL DMF in a 125 mL flask. 1.39 g (10.93 mmol) of 1-butylpyrrolidine (poly(BrEMA)/1-butylpyrrolidine, 1/2 mol/mol) was slowly added dropwise into the flask. The reaction was performed at 80 °C for 48 h. The resulting polymer was precipitated in hexane, followed by extensive washing in hexane multiple times. The solid polymer was dried under vacuum at room temperature for at least 24 h resulting in a yield of 1.5389 g (4.81 mmol) brown solid particles (92.8%). Subsequently, anion exchange metathesis was performed on the dried polymer, poly(MEBPyr-Br), to exchange from Br^- to $TFSI^-$ form (step 3 of Scheme 2 (a)). 8.0905 g (28.2 mmol) of LiTFSI was stirred in 50 mL of DI water and added dropwise into 1.0026 g (3.13 mmol) of poly(MEBPyr-Br) aqueous solution (poly(MEBPyr-Br)/LiTFSI, 1/9 mol/mol). The reaction was carried out at room temperature for 48 h followed by washing with DI water for 72 h. The anion exchanged polymer, poly(MEBPyr-TFSI), was filtered and dried under vacuum in an oven at room temperature for 24 h. Yield: 1.1510 g of solid particles (70.6%). ^{1}H NMR (500 MHz, acetonitrile-d_3, 23 °C) δ (ppm): 4.59-4.07 (s, 2H, N-CH_2-CH_2-O), 3.88-3.42 (s, 6H, N-CH_2-CH_2-CH_2-CH_2-N, N-CH_2-CH_2-CH_2-CH_3), 3.42-3.11 (s, 2H, N-CH_2-CH_2-O), 2.38-2.09 (s, 4H, N-CH_2-CH_2-CH_2-CH_2-N), 1.78-1.62 (s, 2H, N-CH_2-CH_2-CH_2-CH_3), 1.46-1.30 (s, 3H, CH_2-C(CH_3)), 1.16-0.80 (m, 7H, N-CH_2-CH_2-CH_2-CH_3, CH_2-C(CH_3) (NMR, Figure 1). EA calculated: C, 36.92; H, 5.03; N, 5.38; Br, 0.00; S, 12.32; F, 21.90. Found: C, 38.16; H, 5.13; N, 5.04; Br, 0.00; S, 12.32; F, 20.14.

Synthesis of Poly(VBBPyr-TFSI). The synthesis procedure of poly(VBBPyr-TFSI) [VBBPyr = vinylbenzyl butylpyrrolidinium] is shown in in step 2A of Scheme 2(b). An example reaction: 2.0006 g (13.11 mmol) of poly(VBC) was dissolved in 25 mL DMF in a 125 mL flask. 3.34 g (26.25 mol) of 1-butyl pyrrolidine (poly(VBC)/1-butyl pyrrolidine, 1/2 mol/mol) was slowly added

dropwise into the flask. The reaction was carried out at 80 °C for 48 h. The resulting polymer was precipitated in hexane and subsequently washed in hexane multiple times. The solid polymer was dried under vacuum in an oven at room temperature for at least 24 h yielding 4.21 g (15.04 mmol) brown solid particles (114.7%; yield in excess of 100% due to residual solvent). Subsequently, anion exchange metathesis was performed on the dried polymer, poly(VBBPyr-Cl), to exchange from Cl^- to $TFSI^-$ form (step 3 of Scheme 2(b)). 13.8799 g (48.3 mmol) of LiTFSI was stirred in 100 mL of DI water and added dropwise into 1.5033 g (5.37 mmol) of poly(VBBPyr-Cl) aqueous solution (poly(VBBPyr-Cl)/LiTFSI, 1/9 mol/mol). The reaction was carried out at room temperature for 48 h followed by washing with DI water for 72 h. The anion exchanged polymer, poly(VBBPyr-TFSI), was filtered and dried under vacuum in an oven at room temperature for 24 h. Yield: 2.2247 g (4.24 mmol) of solid polymer (79.0%). ^{1}H NMR (500 MHz, acetonitrile-d_3, 23 °C) δ (ppm): 7.39-6.12 (m, 4H, C_6H_4), 4.46-3.74 (m, 2H, C_6H_4-CH_2-N), 3.56-3.06 (s, 4H, N-CH_2-CH_2-CH_2-CH_2-N), 3.06-2.62 (s, 2H, N-CH_2-CH_2-CH_2-CH_3), 2.23-1.06 (m, 11H, N-CH_2-CH_2-CH_2-CH_2-N, CH_2-C*H,* N-CH_2-CH_2-CH_2-CH_3, CH_2-CH, N-CH_2-CH_2-CH_2-CH_3), 1.01-0.72 (s, 3H, N-CH_2-CH_2-CH_2-CH_3) (NMR, Figure 1). EA calculated: C, 43.51; H, 5.00; N, 5.34; Cl, 0.00; S, 12.23; F, 21.73. Found: C, 43.78; H, 5.04; N, 5.49; Cl, 0.00; S, 12.05; F, 21.46.

Synthesis of Poly(VBTMA-TFSI). The synthesis procedure of poly(VBTMA-TFSI) [VBTMA= vinylbenzyltrimethylammonium] is shown in step 2B of Scheme 2(b). An example reaction: 3.0109 g (19.73 mmol) of poly(VBC) was dissolved in 15 mL DMF in a 125 mL flask. 12.91 g (98.28 mol) of 45 wt% trimethylamine aqueous solution (poly(VBC)/trimethylamine, 1/5 mol/mol) was slowly added dropwise into the flask. The reaction was carried out at room temperature for 48 h. The resulting polymer was precipitated in diethyl ether and subsequently

washed in diethyl ether multiple times. The solid polymer was dried under vacuum in an oven at room temperature for at least 24 h yielding 4.8121 g (22.73 mmol) white solid particles (115.2%; yield in excess of 100% due to residual solvent). Subsequently, anion exchange metathesis was performed on the dried polymer, poly(VBTMA-Cl), to exchange from Cl^- to $TFSI^-$ form (step 3 of Scheme 2(b)). 24.3439g (84.80 mmol) of LiTFSI was stirred in 100 mL of DI water and added dropwise into 2.0040 g (9.46 mmol) of poly(VBTMA-Cl) aqueous solution (poly(VBTMA-Cl)/LiTFSI, 1/9 mol/mol). The reaction was carried out at room temperature for 48 h followed by washing with DI water for 72 h. The anion exchanged polymer, poly(VBTMA-TFSI), was filtered and dried under vacuum in an oven at room temperature for 24 h. Yield: 3.1950 g (7.00 mmol) of solid polymer (74.0%). ^{1}H NMR (500 MHz, DMSO-d_6, 23 °C) δ (ppm): 7.53-5.94 (m, 4H, C_6H_4), 4.64-3.77 (m, 2H, C_6H_4-CH_2-N), 3.17-2.39 (s, 9H, N-$(CH_3)_3$), 1.85−0.72 (s, 3H, CH_2-CH, CH_2-CH) (NMR, Figure 1). EA calculated: C, 36.84; H, 3.97; N, 6.14; Cl, 0.00; S, 14.05; F, 24.97. Found: C, 36.97; H, 3.83; N, 6.06; Cl, 0.00; S, 14.02; F, 24.84.

Synthesis of Poly(VBBIm-TFSI). The synthesis procedure of poly(VBBIm-TFSI) [VBBIm= vinylbenzylbutylimidazolium] is shown in step 2C of Scheme 2(b). An example reaction: 3.0046 g (19.69 mmol) of poly(VBC) was dissolved in 35 mL DMF in a 125 mL flask. 12.20 g (98.24 mol) of 1-butylimidazole (poly(VBC)/1-butylimidazole, 1/5 mol/mol) was slowly added dropwise into the flask. The reaction was carried out at 80 °C for 48 h. The resulting polymer was precipitated in hexane and subsequently washed in hexane multiple times. The solid polymer was dried under vacuum in an oven at room temperature for at least 24 h yielding 6.2785 g (22.68 mmol) light yellow solid particles (115.2%; yield in excess of 100% due to residual solvent). Subsequently, anion exchange metathesis was performed on the dried polymer, poly(VBBIm-Cl),

to exchange from Cl^- to $TFSI^-$ form (step 3 of Scheme 2(b)). 18.6270 g (64.9 mmol) of LiTFSI was stirred in 100 mL of DI water and added dropwise into 1.9999 g (7.22 mmol) of poly(VBBIm-Cl) aqueous solution (poly(VBBIm-Cl)/LiTFSI, 1/9 mol/mol). The reaction was carried out at room temperature for 48 h followed by washing with DI water for 72 h. The anion exchanged polymer, poly(VBBIm-TFSI), was filtered and dried under vacuum in an oven at room temperature for 24 h. Yield: 3.2991g of solid polymer (87.6%). ^{1}H NMR (500 MHz, DMSO-d_6, 23 °C) δ (ppm): 9.39-9.09 (s,1H, N-C*H*=N), 7.88-7.59 (s, 2H, N-C*H*=C*H*-N), 7.57-6.01 (m, 4H, C_6H_4), 5.41-4.79 (m, 2H, C_6H_4-CH_2-N), 4.39-3.86 (s, 2H, N-CH_2-CH_2-CH_2-CH_3), 1.83−1.56 (m, 3H, CH_2-C*H,* N-CH_2-CH_2-CH_2-CH_3), 1.56−0.93 (m, 4H, CH_2-CH, N-CH_2-CH_2-CH_2-CH_3), 0.93-0.58 (s, 3H, N-CH_2-CH_2-CH_2-CH_3) (NMR, Figure 1). EA calculated: C, 41.46; H, 4.06; N, 8.06; Cl, 0.00; S, 12.30; F, 21.86. Found: C, 41.47; H, 4.03; N, 7.94; Cl, 0.00; S, 12.41; F, 21.68.

Scheme 2. Synthesis of PILs: (a) poly(MEBPyr-TFSI); (b) poly(VBX^+-TFSI), X^+ = various cations: (A) BPyr, (B) TMA, (C) BIm.

(a)

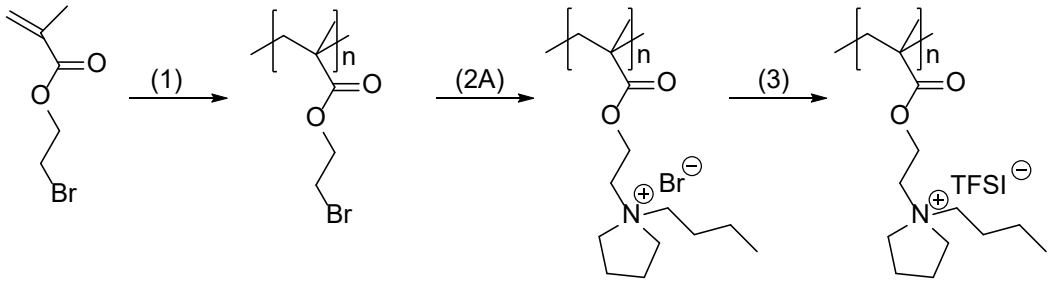

(b)

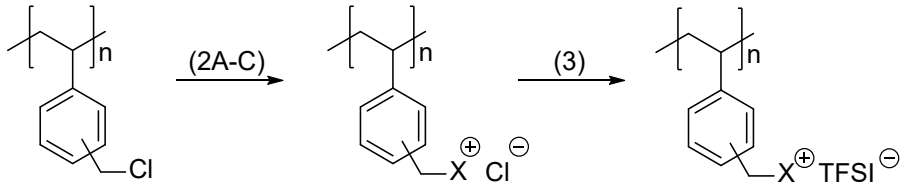

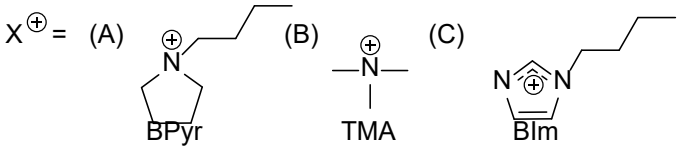

(1) CTA, THF, AIBN, 70 °C, 5h; (2A) 1-butylpyrrolidine, DMF, 80 °C, 48h; (2B) trimethylamine (aqueous), DMF, room temperature, 48h; (2C) 1-butylimidazole, DMF, 80 °C, 48h; (3) LiTFSI, H_2O, room temperature, 48 h

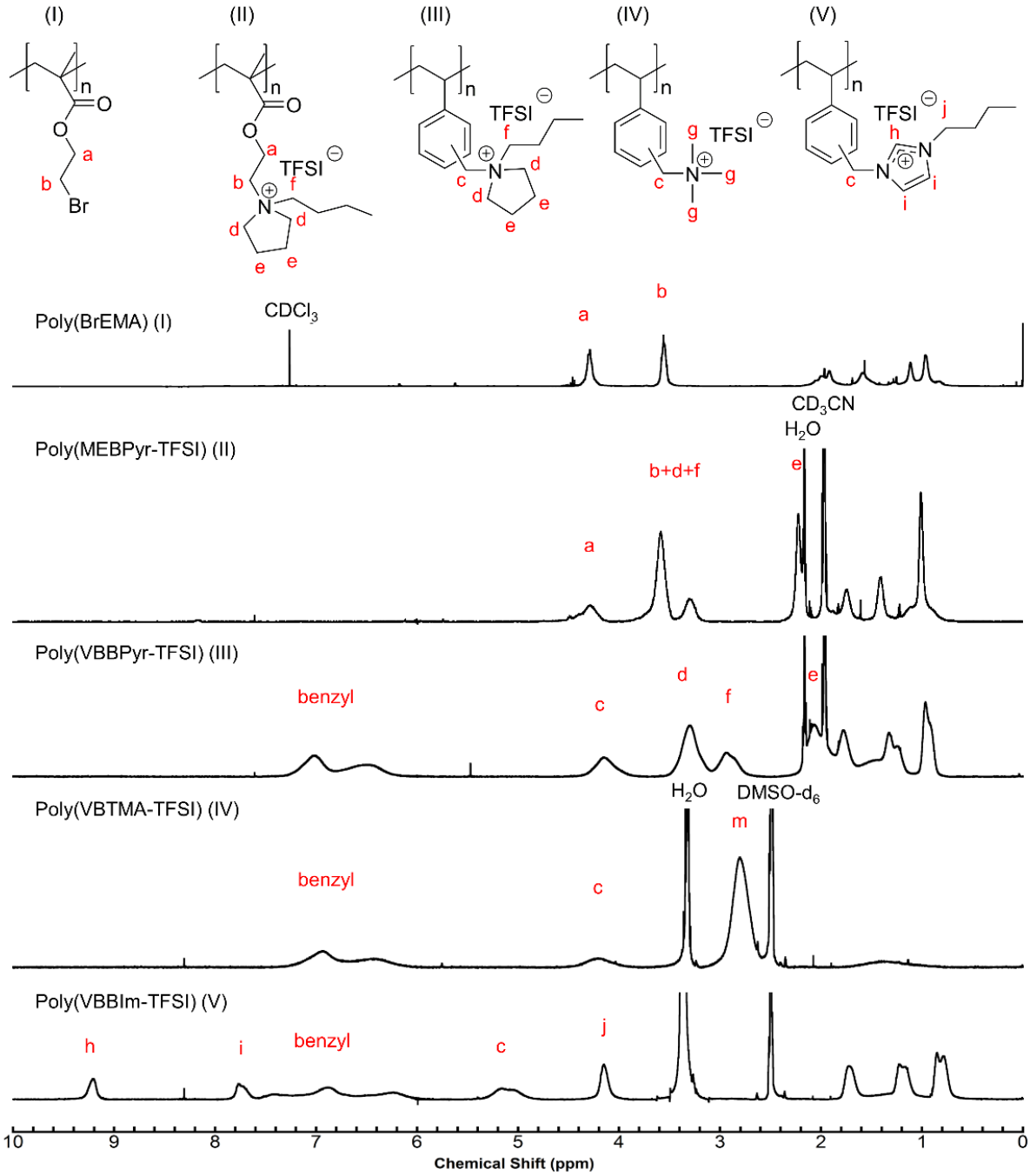

Figure 1. ^{1}H NMR spectra for (I) poly(BrEMA), (II) poly(MEBPyr-TFSI), (III) poly(VBBPyr-TFSI), (IV) poly(VBTMA-TFSI), (V) poly(VBBIm-TFSI).

Carbonization. Carbonization of PILs and PAN were carried out in quartz tube furnace. Carbonization was performed at 900 °C, as this was reported as the threshold temperature for the

development of a large surface area and low resistance.[39] An example reaction included placing 1.0014 g of poly(VBBPyr-TFSI) into a quartz combustion boat and heating in the tube furnace under nitrogen environment (flow rate: 300 mL/min) with a controlled ramp rate of 10 °C/min up to 900 °C, where the temperature was held constant for 2 h. Additional carbonizations of poly(MEBPyr-TFSI), poly(VBBIm-TFSI), poly(VBTMA-TFSI), and PAN followed the same procedure as poly(VBBPyr-TFSI).

Characterization. The molecular weight and molecular weight distribution of poly(BrEMA) was performed with gel permeation chromatography (GPC) with a Waters GPC system (breeze 2) equipped with a THF Styragel column (Styragel@HR 5E, effective separation of molecular weight range: 2 to 4000 kg mol^{-1}) and a 2414 refractive index (RI) detector. GPC was calibrated with polystyrene standards (M_w: 2.97 to 983 kg mol^{-1}) and the experiment was performed at 40 °C under a flow rate of 1.0 mL/min for the mobile phase (THF). Chemical analysis was performed with ^1H NMR spectroscopy (Varian Inova 500 MHz spectrometer) at 23 °C with various NMR solvents. ^1H NMR spectra of BrEMA and poly(BrEMA) were collected referencing to $CDCl_3$ at 7.27 ppm. ^1H NMR spectra of poly(MEBPyr-TFSI) and poly(VBBPyr-TFSI) were collected referencing to acetonitrile-d_3 at 1.94 ppm. ^1H NMR spectra of the remaining polymers were collected referencing to DMSO-d_6 at 2.50 ppm. Elemental analysis was performed by Atlantic Microlab, Inc. in Norcross, GA. Infrared spectroscopy was performed at room temperature by a Fourier transform infrared (FTIR) spectrometer (Nicolet 6700 Series; Thermo Electron Corporation) using a single reflection diamond ATR accessory (Specac; Quest). All infrared spectra were collected using a liquid nitrogen-cooled mercury-cadmium-telluride (MCT) detector at 32 scans per spectrum and a resolution of 4 cm^{-1}. The spectra were corrected with a background subtraction of the spectrum of

the bare ATR crystal. Differential scanning calorimetry (DSC, TA Instruments, Q200) was performed to determine glass transition temperatures (T_gs). The measurements were collected under nitrogen environment (50 mL/min) using a method of heat/cool/heat at a heating/cooling rate of 10 °C/min over a temperature range of -140 to 180 °C. T_gs were determined using the mid-point method on the second heating cycle thermogram. Thermal gravimetric analysis (TGA; TA Instruments, Q50) was performed to determine thermal degradation temperatures (T_ds). The measurements were collected under nitrogen environment (60 mL/min) at a heating rate of 10 °C/min over the temperature range of 25 to 900°C. The degradation temperature was determined at 5% weight loss.

Optical images were collected using a Zeiss Axiophot optical microscope with a 5X aperture. Higher magnification images were collected by scanning electron microscopy (SEM, FEI Quanta 600 FE-SEM) and transmission electron microscopy (TEM, JEOL JEM-2010). SEM images were taken at 20 kV. Samples were loaded on carbon coated stubs and coated by 6 mm sputtering Pt-Pd alloy prior to obtaining images. TEM images were taken at an acceleration voltage of 200 kV with LaB_6 filament. Samples were prepared in ethanol with sonication for 10 mins (40% amplitude, QSONICA Q125 sonicator).

X-ray diffraction (XRD) patterns were recorded on a Bruker-AXS D8 Advanced Bragg-Brentano X-ray powder diffractometer using Cu-K_α radiation ($\lambda = 0.154$ nm). Raman spectroscopy was performed using Horiba Jobin-Yvon LabRam HR Raman confocal microscope with 632.8 nm laser excitation. The intensity ratio of D band to G band (I_D/I_G) was calculated using the peak height of D and G band of deconvoluted peaks using Lorentzian profiles. X-ray photoelectron spectroscopy (XPS) was performed on an Omicron XPS/UPS system with Argus detector using Omicron's DAR 400 dual Mg X-ray source.

Nitrogen adsorption-desorption isotherms were collected at 77 K using Quantachrome's Autosorb-iQ instrument. The surface area and pore size distribution were calculated using the Brunauer-Emmett-Teller (BET) model and density functional theory (DFT).

RESULTS AND DISCUSSION

PILs: Carbon Precursors. Four PILs were synthesized with various backbone/cation pairings (backbones: ethyl methacrylate, styrene; covalently attached cations: butylpyrrolidinium, trimethylammonium, butylimidazolium) as carbon precursors. Functionalization reactions were performed on non-ionic polymer precursors, poly(BrEMA) and poly(vinylbenzyl chloride), following a literature procedure[48] to achieve PILs (shown in Scheme 2). The resulting functionalized polymers, poly(MEBPyr-Br), poly(VBBPyr-Cl), poly(VBTMA-Cl), and poly(VBBIm-Cl) were found to be hygroscopic and water-soluble. Therefore, water was chosen as solvent for anion exchange metathesis. The chemical structures of poly(BrEMA) and TFSI-form PILs were confirmed by ^{1}H NMR, where the PILs were calculated to be approximately fully functionalized (Figure 1). EA results confirmed that the anion exchange metatheses were successful and highly efficient, as the compositions of the anion exchanged PILs closely match the theoretical compositions, and the bromide and chloride residues were negligibly small for methacrylate and styrene based PILs, respectively.

Infrared ATR spectra (Figure 2) further confirmed the chemistry of the PILs. The characteristic infrared bands of the TFSI anion were found in all PILs (*i.e.*, SO_2 stretching bands: 1346 cm^{-1},1053 cm^{-1}; CF_3 stretching band: 1177, 1131 cm^{-1}; S-N-S stretching bands: 789 cm^{-1} and 741 cm^{-1}; antisymmetric CF_3 bending band: 762 cm^{-1}), similar to TFSI anion assignments in literature.[49] The

chemical structures of the polymer backbones were also confirmed by the infrared spectra: C=O stretching (1727 cm^{-1}) from carboxyl groups and C=C stretching (1561 cm^{-1}) from aromatic ring.

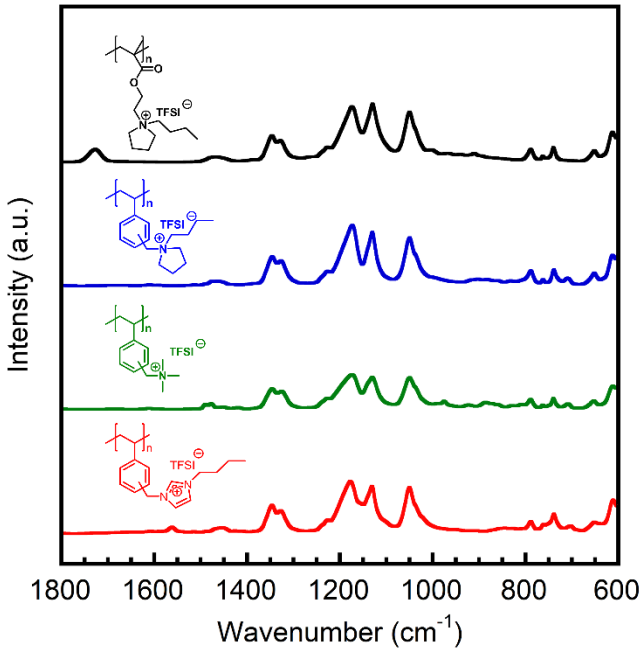

Figure 2. Infrared spectra of PILs: poly(MEBPyr-TFSI) (black), poly(VBBPyr-TFSI) (blue), poly(VBTMA-TFSI) (green), and poly(VBBIm-TFSI) (red).

DSC thermograms of all TFSI-form PILs are shown in Figure 3(a) and the glass transition temperatures (T_gs) are listed in Table 1. Note that there is an 81 °C difference in T_gs, where poly(VBTMA-TFSI) has the highest T_g of 90 °C and poly(VBBIm-TFSI) has the lowest T_g of 9 °C. Cation type (same anion and same backbone) shows a strong influence on T_g. The sequence of T_gs with different cation type is as follows: butylimidazolium < butylpyrrolidinium < trimethylammonium. More free volume is created by the butylimidazolium and butylpyrrolidinium cations compared to trimethylammonium cation, resulting in a depression of T_g. When comparing the thermograms of poly(VBBIm-TFSI) and poly(VBBPyr-TFSI), the alkyl chain and ring-size effects were deconvoluted by the presence of the same butyl group and five-membered ring on

both cations. The difference in T_g may be a result of the unsaturated structure of the imidazolium cation, where the charge delocalization introduced by the benzylic butylimidazolium cation may change the cation-anion interactions and lower the T_g. The polymer backbone type appears to have less of an influence on T_g, *i.e.*, analogous T_gs were observed for poly(MEBPyr-TFSI) and poly(VBBPyr-TFSI) (*i.e.,* butylpyrrolidinium-PILs with styrene and methacrylate backbones).

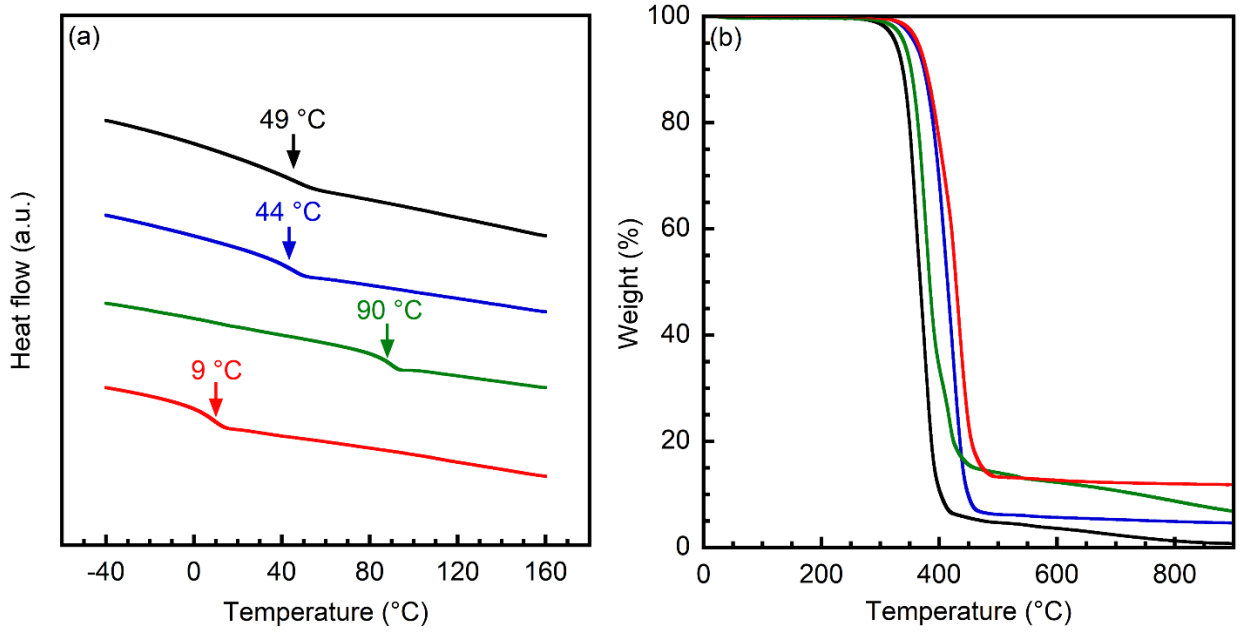

Figure 3. (a) DSC thermograms and (b) TGA thermograms of PILs: poly(MEBPyr-TFSI) (black), poly(VBBPyr-TFSI) (blue), poly(VBTMA-TFSI) (green), and poly(VBBIm-TFSI) (red).

TGA thermograms of all TFSI-form PILs are shown in Figure 3(b) and the thermal decomposition temperatures (T_ds) are listed in Table 1. Previous studies indicate that anion type significantly affects the thermal stability of PILs.[47] T_ds confirmed that TFSI-form PILs are highly thermally stable, where TFSI-exchanged PILs have an average T_d of 340 °C. TFSI-exchanged PILs are found to undergo a one-step decomposition *via* sulfur dioxide release rather than dealkylation or proton transfer and exhibit a higher decomposition temperature compared to other anions.[50] In

this study, by eliminating the effect of anion type (same anion for all PILs), the effect of cation type on thermal stability was investigated. It is generally accepted that pyrrolidinium cation has higher thermal stability than imidazolium cation and tetraalkyl ammonium cation for their analogous ionic liquids.[51] However, the thermal stability results of these PILs were inconsistent with previous results on ionic liquids. T_d was found to correlate with cation type as follows: butylpyrrolidinium < trimethylammonium < butylimidazolium. Vinylbenzyl and ethyl methacrylate backbones were compared for one cation type (butylpyrrolidinium) and minimal difference was observed between the two T_ds.

Table 1. Thermal decomposition temperatures (T_ds) and glass transition temperatures (T_gs) of PILs.

Polymer	T_d (°C)	T_g (°C)
poly(MEBPyr-TFSI)	326	49
poly(VBBPyr-TFSI)	330	44
poly(VBTMA-TFSI)	341	90
poly(VBBIm-TFSI)	364	9

Carbons Derived from PILs. Carbon materials were achieved from all PILs, which provides evidence that PILs can be successfully employed as carbon precursors. Table 2 lists the measured properties of PAN- and PIL-derived carbons. The calculated mass yields (Table 2) vary with both cation and backbone types. When comparing the carbon yields of poly(MEBPyr-TFSI) and poly(VBBPyr-TFSI) with the same butylpyrrolidinium cation, the styrene backbone provided a higher carbon yield relative to the methacrylate backbone. It was noted that unsaturated carbon atoms in sp^2 or sp hybrid state can stay in the resulting carbon as condensable groups and will contribute to the formation of graphitic structure.[39] As a result, the higher yield can be attributed to the extra sp^2 hybridized carbons from the aromatic structure. The methacrylate backbone was also reported to undergo depolymerization with over 90% monomer yield (higher than styrene

backbone), which further explains the lower carbon yield of compared to styrene-based PILs.[52] Cation type also showed a considerable impact on carbon yield. For styrene-based PILs, carbon yield relative to cation type follows the order: butylpyrrolidinium < trimethylammonium < butylimidazolium. The higher carbon yield of poly(VBBIm-TFSI) may result from the incorporation of the extra unsaturated carbon atoms of butylimidazolium cation. In contrast, PAN achieved the highest carbon yield (30.3 %), as a result of the cyclization initiated by the nitrile group and the formation of a ladder structure during the pyrolysis process.[53] This process lowers the possibility of molecular disorientation and retains a higher mass yield by converting the volatile linear structure into a ring conformation.[28] Therefore, the carbon yield of PIL-derived carbons may be further improved by nitrile substitution onto the polymer backbone and/or cation, as suggested in literature.[35, 38]

Table 2. Characterization of PIL-derived carbons and PAN-derived carbon.

Polymer[a]	Mass yield (wt %)	I_D/I_G[b]	N_{XPS} (wt %)	N retention (wt %)	N state (%)[c]		
					N_1	N_2	N_3
poly(MEBPyr-TFSI)	6.4	1.41	1.30	1.7	33.5	66.5	0
poly(VBBPyr-TFSI)	7.3	1.42	2.20	2.9	23.7	76.3	0
poly(VBTMA-TFSI)	13.9	1.40	1.09	2.5	20.1	79.9	0
poly(VBBIm-TFSI)	22.1	1.41	2.70	7.5	32.3	57.8	9.9
PAN	30.3	1.43	5.61	6.4	36.3	59.9	3.8

[a] PIL structures are shown in Scheme 1. [b] Intensity ratio of D band to G band (I_D/I_G) of the carbon materials derived from PILs and PAN were calculated from deconvoluted Raman spectra by Lorentz peak fitting. [c] Binding energy: pyridinic N (N_1): 398.3 ± 0.1 (eV); graphitic N (N_2): 400.9 ± 0.1 (eV); oxidized N (N_3): 403.7 (eV).

In addition to the carbon yield, the appearances of the resulting carbon materials from PILs (Figure 4(a) and Figure S1, Supporting Information) and PAN (Figure 4(d)) vary significantly. Carbonization of PAN results in black powder, similar to what has been observed in literature.[28]

Carbonization of PILs results in something quite unexpected: carbon sheets. The difference in appearance can be attributed to the different carbonization mechanisms of PILs and PAN. The PILs melted in the process of heating due to their low T_gs,[44] which formed films at the bottom of the quartz boats and further resulted in carbon sheets. The carbon sheets possessed a metallic luster, suggesting that a higher graphitic content may have been achieved during pyrolysis. Selected SEM (Figure 4(b) and 4(e), and Figure S2, Supporting Information) and TEM images (Figure 4(c) and 4(f), and Figure S3, Supporting Information) further showed the difference between the morphology of PIL- and PAN-derived carbons. The SEM image of PAN-derived carbon (Figure 4(e)) shows a structure consisting of an aggregation of particles with a broad particle size distribution, whereas the surfaces of PIL-derived carbons (Figure 4(b) and Figure S2, Supporting Information) were flat and relatively smooth. TEM images of PIL-derived carbons (Figure 4(c) and Figure S3, Supporting Information) exhibited compact multi-layer structures, while PAN-derived carbon (Figure 4(f)) possessed a relatively thin-layer morphology. The morphologies did not vary significantly when comparing styrene-based PILs with different cation types, indicating that the cation type has a minor influence on the morphology.

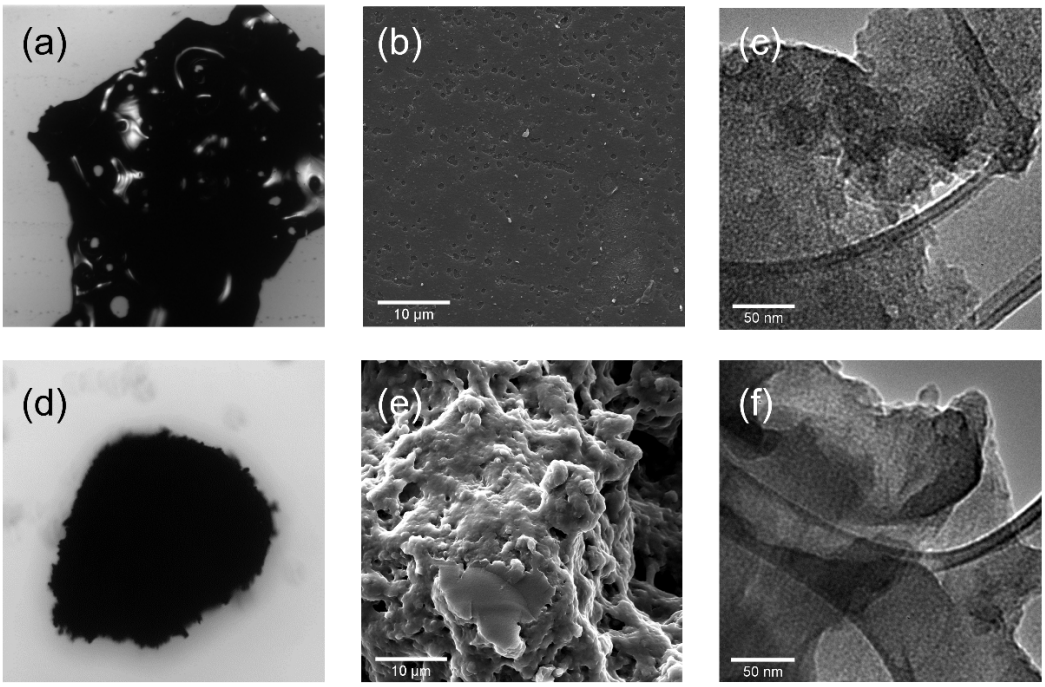

Figure 4. Selected microscopic images of PIL-derived and PAN-derived carbons. Top row: (a) optical image, (b) SEM image, (c) TEM image of poly(VBBIm-TFSI)-derived carbon. Bottom row: (d) optical image, (e) SEM image, (f) TEM image of PAN-derived carbon.

XRD patterns (Figure 5(a)) revealed the phases and structures of the PIL and PAN-derived carbons. Reflection bands at 26° ((0 0 2) plane reflection) and 44° ((1 0 0) plane reflection) were observed in both PAN- and PIL-derived carbons, suggesting the existence of graphitic structure.[28] Raman spectra of the carbon products derived from PILs and PAN (Figure 5(b)) exhibited two distinct peaks at 1320 cm^{-1} (D band) and 1596 cm^{-1} (G band). The G band is attributed to the E_{2g} symmetric vibration of graphitic carbon structure, while the D band is related to the A_{1g} vibration of structural defects and disordered structure of carbon materials.[23] The intensity ratio (I_D/I_G) (shown in Table 2), which reflects the degree of graphitization, was calculated using the intensity of D and G band. Relative to PAN-derived carbon, PIL-derived carbons possessed slightly smaller I_D/I_G ratio, which may reveal higher graphitization extent. The increase in graphitization extent

may be a result of the anion-to-anion correlations and molecular templating mechanism induced by the large TFSI counterion.[35, 54, 55]

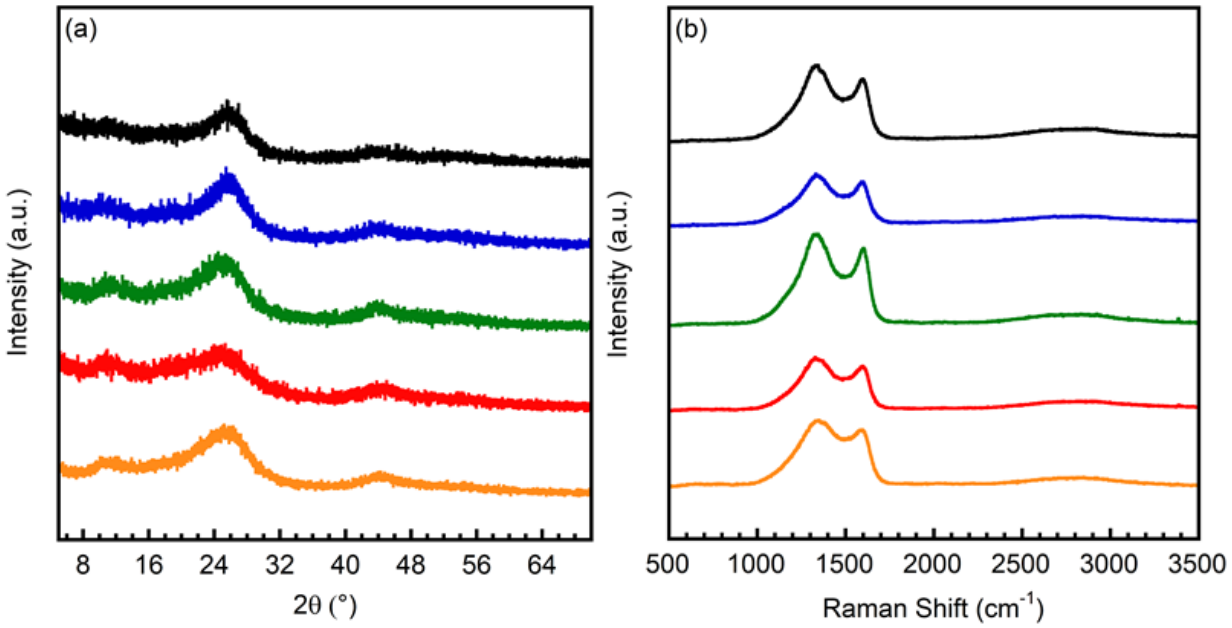

Figure 5. (a) XRD patterns and (b) Raman spectra of carbon derived from: poly(MEBPyr-TFSI) (black), poly(VBBPyr-TFSI) (blue), poly(VBTMA-TFSI) (green), poly(VBBIm-TFSI) (red) and PAN (orange).

XPS spectra (Figure 6) reveals the surface chemistry of the carbon materials. PIL-derived carbons exhibit characteristic peaks at 284.8 eV (C 1s), 398.6 eV (N 1s), 532.3 eV (O 1s) and 164.5 eV (S 2p) confirming the existence of C, N, O and S elements, while PAN-derived carbon only contains C, N, and O elements. The surface elemental compositions are summarized in Table S1 (Supporting Information). PIL-derived carbons possess nitrogen contents (Table 2) of 1.30%, 2.20%, 1.09%, 2.70% for poly(MEBPyr-TFSI), poly(VBBPyr-TFSI), poly(VBTMA-TFSI), and poly(VBBIm-TFSI), respectively, with a PIL precursor nitrogen content of 5.04%, 5.49%, 6.06%, 7.94%, respectively, whereas PAN-derived carbon possess a higher nitrogen content of 5.61% with a higher precursor nitrogen content of 26.40%. The relatively high nitrogen content of PAN-

derived carbon might be a result of the cyclization mechanism of the nitrile group in polymer backbone, which promotes the incorporation of nitrogen atoms by forming a more thermally stable ladder conformation.[53] To better understand the effective nitrogen yield, the percentage of nitrogen retention (Table 2) was calculated by the ratio of nitrogen content in the resulting carbons to their polymer precursor nitrogen content. Poly(VBBIm-TFSI) obtained the highest nitrogen retention among the resulting nitrogen-doped carbons with a nitrogen retention of 7.5%, higher that the 6.4% nitrogen retention of PAN-derived carbon. The higher nitrogen retention of poly(VBBIm-TFSI) suggests that the nitrogen and carbon atoms in the unsaturated cyclic butylimidazolium cation may positively influence the nitrogen integration similar to nitrile groups. This is further confirmed by the relatively low nitrogen retention of PIL-derived carbons with aliphatic cation groups. Therefore, cation type significantly affects the nitrogen fixation and the nitrogen content might be further improved by the selection of various cation and anion pairings.

The chemical state of the nitrogen atoms was identified by the deconvolution of high-resolution nitrogen XPS spectra. The nitrogen can be divided into two categories: surface bounded nitrogen (nitro and amine groups) and structural incorporated nitrogen (pyridinic N, pyrrolic N, and quaternary N).[44] The pyridinic N and pyrrolic N may induce structural defects into the carbon network and decrease the degree of graphitization, while the quaternary N will be integrated to form sp^2 graphitic layers. In this study, the deconvolution of N 1s depicted characteristic peaks of pyridinic N (398.3 ± 0.1 eV) and quaternary N (400.9 ± 0.1 eV) indicates that nitrogen atoms were structurally integrated into the carbon matrix and predominately in pyridinic and quaternary forms.[23, 56] Oxidized N (403.7 eV) were found in poly(VBBIm-TFSI) and PAN-derived carbons, which represents the nitro groups impurities developed on the surface. The composition of different nitrogen components in all carbon materials are listed in Table 2. PIL-derived carbons

contain higher composition of quaternary N (graphitic N) compared to PAN-derived carbon. This is attributed to the molecular templating mechanism of the large TFSI anion of the PIL precursors as described previously.[35, 54] The surface chemistry structure and composition of N component varied with different cations on styrene-based PIL precursors. Graphitic N content in carbons increases with different polymer cation type: butylimidazolium < butylpyrrolidinium < trimethylammonium. Poly(VBTMA-TFSI) derived carbon consisted of 79.9% graphitic N, which is consistent with the highest degree of graphitization from Raman spectra. Styrene backbone resulted in higher graphitic N content compared to methacrylate backbone for polymers with butylpyrrolidinium cation, which might be attributed to the aromatic configuration contribution in the formation of sp^2 graphene layers. Additionally, with the TFSI anion, sulfur was also introduced into the PIL-derived carbons (Table S1, Supporting Information). Therefore, nitrogen and sulfur bifunctionalized carbon materials were achieved.

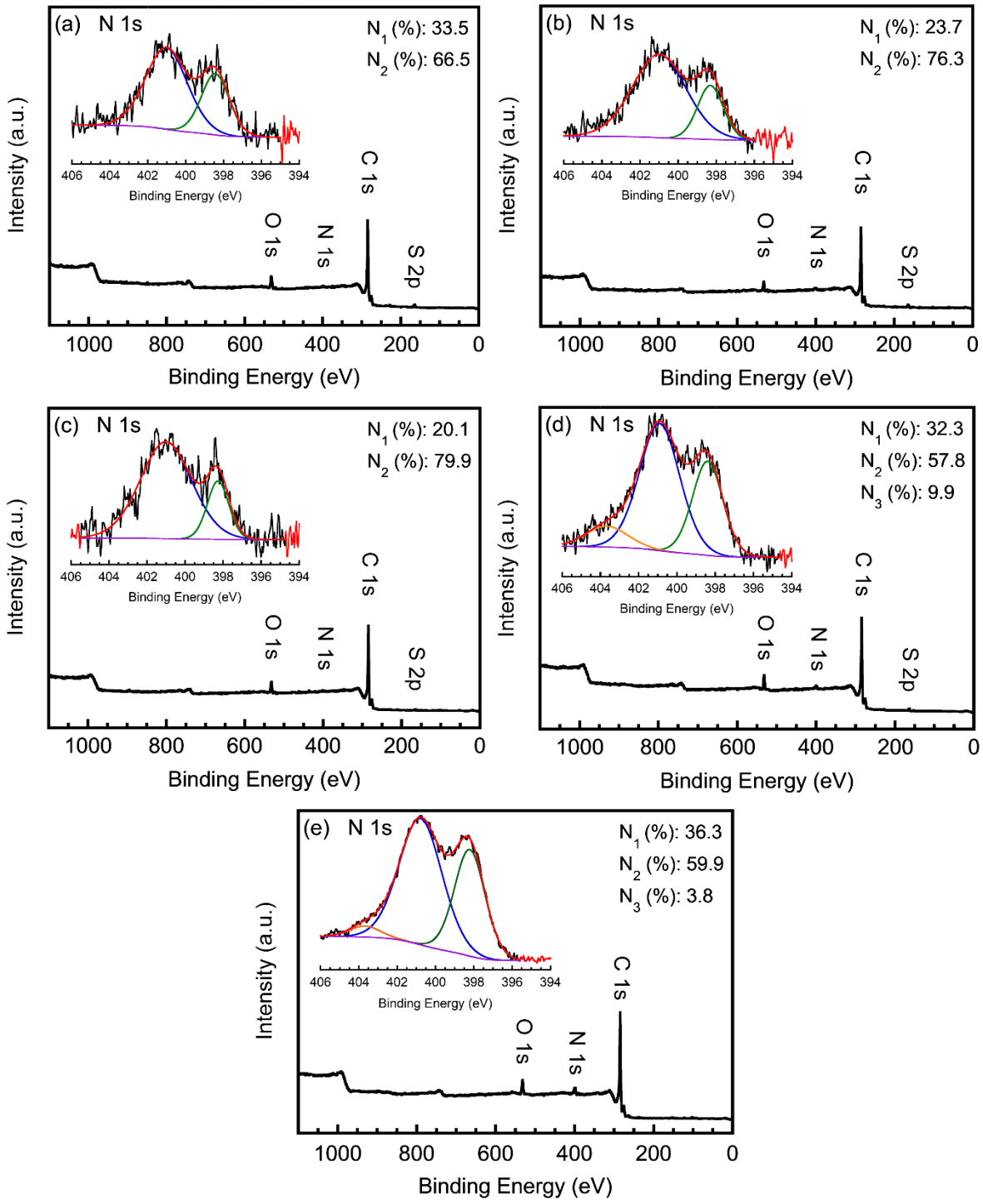

Figure 6. XPS spectra of the carbon derived from: (a) poly(MEBPyr-TFSI), (b) poly(VBBPyr-TFSI), (c) poly(VBTMA-TFSI), (d) poly(VBBIm-TFSI) and (e) PAN.

Significant surface area differences were observed among all investigated carbon materials. Of the PIL-derived carbons, poly(VBBIm-TFSI)-derived carbon showed a relatively high specific surface area (S_{BET}) of 590.4 m^2/g, while other PIL-derived carbons are considered nonporous with S_{BET} less than 100 m^2/g, indicating that cation type of polymer precursors has a profound influence on the surface area. The sharp difference in textural properties among different cation types might be assigned to the possible crosslinking effect offered by the unsaturated carbon on imidazolium cation to form a stable network before the decomposition of TFSI anion.[43] Nitrogen sorption isotherm of poly(VBBIm-TFSI) derived carbon (Figure S4, Supporting Information) exhibited a combined Type I/Type IV isotherm with a steep N_2 uptake at low relative pressure ($p/p_0<0.1$), suggesting the primary presence of microporosity following the definition by Brunauer.[57] A small portion of mesopores also exist due to the detection of the type-H4 hysteresis loop at the relative pressure between 0.4 to 0.8. The calculated pore distribution was 88.2% micropores by surface area with half pore size less than 0.7 nm, which is determined to be ultramicroporosity. The formation of this ultramicroporous structure may be due to the molecular templating mechanism of large anion TFSI as described in literature.[35, 54] Different from poly(VBBIm-TFSI)-derived carbon, PAN-derived carbon achieved a low S_{BET}. The difference was attributed to the thermal decomposition of TFSI anion moiety. TFSI anion might be trapped in the carbon network at a lower temperature due to its relatively high thermal stability and will form a microporous structure by the one-step decomposition.[24]

CONCLUSIONS

A series of PILs with various backbone/cation pairings (backbones: ethyl methacrylate, styrene; covalently attached cations: butylpyrrolidinium, trimethylammonium, butylimidazolium) were synthesized as polymer precursors for carbon materials. Thermal properties of PILs were

investigated by cation type and polymer backbone type, where both the glass transition temperature (butylimidazolium < butylpyrrolidinium < trimethylammonium) and the thermal degradation temperature (butylpyrrolidinium < trimethylammonium < butylimidazolium) varied by cation type. Nitrogen-doped carbons were successfully derived from these PILs and compared to PAN-derived carbon. Carbon sheets with metallic luster were observed with PIL-derived carbons, while PAN-derived carbon possessed the appearance of black solid powder. Pyridinic N and graphitic N were found in all carbon materials, indicating that N atoms were structurally integrated into the carbon matrix. Among the PIL-derived carbons, poly(VBTMA-TFSI)-derived carbon showed the highest graphitization extent and graphitic nitrogen content. Cation type significantly impacted carbon yield, graphitization extent, surface chemistry and surface area of the resulting carbon materials, where poly(VBBIm-TFSI) achieved the highest surface area of 590.4 m^2/g. The design of PIL chemistry based on cation and polymer backbone effects offers the opportunity to optimize the characteristics of PIL-derived nitrogen-doped graphitic carbon for its subsequent implications in energy storage applications.

ACKNOWLEDGEMENTS

The work is supported in part by the U.S. Army Research Office under grant number W911NF-14-0310 and the National Science Foundation under award no. CBET-1703645.

SUPPORTING INFORMATION

Additional data related to this article is available free of charge *via* the Internet at ….

REFERENCES

1 E. Frackowiak and F. Beguin, *Carbon* **39:**937-950 (2001).

2 G. P. Wang, L. Zhang and J. J. Zhang, *Chem Soc Rev* **41:**797-828 (2012).

3 W. Zhang, S. Zhu, R. Luque, S. Han, L. Hu and G. Xu, *Chem Soc Rev* **45:**715-752 (2016).

4 P. Simon and Y. Gogotsi, *Nat Mater* **7:**845-854 (2008).

5 A. G. Pandolfo and A. F. Hollenkamp, *J Power Sources* **157:**11-27 (2006).

6 Y. P. Zhai, Y. Q. Dou, D. Y. Zhao, P. F. Fulvio, R. T. Mayes and S. Dai, *Adv Mater* **23:**4828-4850 (2011).

7 E. Frackowiak, *Phys Chem Chem Phys* **9:**1774-1785 (2007).

8 D. Lozano-Castello, D. Cazorla-Amoros, A. Linares-Solano, S. Shiraishi, H. Kurihara and A. Oya, *Carbon* **41:**1765-1775 (2003).

9 J. P. Paraknowitsch and A. Thomas, *Energy Environ Sci* **6:**2839-2855 (2013).

10 M. Seredych, D. Hulicova-Jurcakova, G. Q. Lu and T. J. Bandosz, *Carbon* **46:**1475-1488 (2008).

11 D. Hulicova-Jurcakova, M. Seredych, G. Q. Lu and T. J. Bandosz, *Adv Funct Mater* **19:**438-447 (2009).

12 H. M. Jeong, J. W. Lee, W. H. Shin, Y. J. Choi, H. J. Shin, J. K. Kang and J. W. Choi, *Nano Lett* **11:**2472-2477 (2011).

13 C. O. Ania, V. Khomenko, E. Raymundo-Pinero, J. B. Parra and F. Beguin, *Adv Funct Mater* **17:**1828-1836 (2007).

14 Z. Li, Z. W. Xu, X. H. Tan, H. L. Wang, C. M. B. Holt, T. Stephenson, B. C. Olsen and D. Mitlin, *Energy Environ Sci* **6:**871-878 (2013).

15 J. Wei, D. D. Zhou, Z. K. Sun, Y. H. Deng, Y. Y. Xia and D. Y. Zhao, *Adv Funct Mater* **23:**2322-2328 (2013).

16 D. Hulicova-Jurcakova, M. Kodama, S. Shiraishi, H. Hatori, Z. H. Zhu and G. Q. Lu, *Adv Funct Mater* **19:**1800-1809 (2009).

17 D. Guo, R. Shibuya, C. Akiba, S. Saji, T. Kondo and J. Nakamura, *Science* **351:**361-365 (2016).

18 K. Gong, F. Du, Z. Xia, M. Durstock and L. Dai, *Science* **323:**760-764 (2009).

19 F. Su, C. K. Poh, J. S. Chen, G. Xu, D. Wang, Q. Li, J. Lin and X. W. Lou, *Energy Environ Sci* **4:**717-724 (2011).

20 D. Hulicova, J. Yamashita, Y. Soneda, H. Hatori and M. Kodama, *Chem Mat* **17:**1241-1247 (2005).

21 Y. Deng, Y. Xie, K. Zou and X. Ji, *J Mater Chem A* **4:**1144-1173 (2016).

22 S. G. Zhang, M. S. Miran, A. Ikoma, K. Dokko and M. Watanabe, *J Am Chem Soc* **136:**1690-1693 (2014).

23 L. Wang, Z. Y. Gao, J. L. Chang, X. Liu, D. P. Wu, F. Xu, Y. M. Guo and K. Jiang, *ACS Appl Mater Interfaces* **7:**20234-20244 (2015).

24 J. Gong, H. Lin, M. Antonietti and J. Yuan, *J Mater Chem A* **4:**7313-7321 (2016).

25 J. Y. Yuan, A. G. Marquez, J. Reinacher, C. Giordano, J. Janek and M. Antonietti, *Polym Chem* **2:**1654-1657 (2011).

26 J.-H. Park, Y.-W. Ju, S.-H. Park, H.-R. Jung, K.-S. Yang and W.-J. Lee, *J Appl Electrochem* **39:**1229-1236 (2009).

27 M. Zhong, E. K. Kim, J. P. McGann, S.-E. Chun, J. F. Whitacre, M. Jaroniec, K. Matyjaszewski and T. Kowalewski, *J Am Chem Soc* **134:**14846-14857 (2012).

28 A. V. Korobeinyk, R. L. D. Whitby and S. V. Mikhalovsky, *Eur Polym J* **48:**97-104 (2012).

29 T. N. Chi and D. P. Kim, *J Mater Chem* **21:**14226-14230 (2011).

30 K. M. Meek and Y. A. Elabd, *J Mater Chem A* **3:**24187-24194 (2015).

31 V. I. Parvulescu and C. Hardacre, *Chem Rev* **107:**2615-2665 (2007).

32 P. Kubisa, *Prog Polym Sci* **29:**3-12 (2004).

33 M. Armand, F. Endres, D. R. MacFarlane, H. Ohno and B. Scrosati, *Nat Mater* **8:**621-629 (2009).

34 J. P. Paraknowitsch, J. Zhang, D. S. Su, A. Thomas and M. Antonietti, *Adv Mater* **22:**87-92 (2010).

35 J. S. Lee, X. Q. Wang, H. M. Luo, G. A. Baker and S. Dai, *J Am Chem Soc* **131:**4596-+ (2009).

36 Z.-L. Xie and D. S. Su, *Eur J Inorg Chem* **2015:**1137-1147 (2015).

37 Q. Yang, Z. Zhang, X.-G. Sun, Y.-S. Hu, H. Xing and S. Dai, *Chem Soc Rev* **47:**2020-2064 (2018).

38 J. P. Paraknowitsch and A. Thomas, *Macromol Chem Physic* **213:**1132-1145 (2012).

39 J. Y. Yuan, C. Giordano and M. Antonietti, *Chem Mater* **22:**5003-5012 (2010).

40 T.-P. Fellinger, A. Thomas, J. Yuan and M. Antonietti, *Advanced Materials (Deerfield Beach, Fla)* **25:**5838-5854 (2013).

41 J. Y. Yuan, H. Schlaad, C. Giordano and M. Antonietti, *Eur Polym J* **47:**772-781 (2011).

42 D. Kuzmicz, P. Coupillaud, Y. Men, J. Vignolle, G. Vendraminetto, M. Ambrogi, D. Taton and J. Y. Yuan, *Polymer* **55:**3423-3430 (2014).

43 Q. Zhao, T. P. Fellinger, M. Antonietti and J. Y. Yuan, *J Mater Chem A* **1:**5113-5120 (2013).

44 M. Einert, C. Wessel, F. Badaczewski, T. Leichtweiss, C. Eufinger, J. Janek, J. Y. Yuan, M. Antonietti and B. M. Smarsly, *Macromol Chem Physic* **216:**1930-1944 (2015).

45 J. Gao, C. He, J. Liu, P. Ren, H. Lu, J. Feng, Z. Zou, Z. Yin, X. Wen and X. Tan, *Catalysis Science & Technology* **8:**1142-1150 (2018).

46 Y. Men, M. Ambrogi, B. Han and J. Yuan, *International Journal of Molecular Sciences* **17:**532 (2016).

47 Y. Ye and Y. A. Elabd, *Polymer* **52:**1309-1317 (2011).

48 K. M. Meek, J. R. Nykaza and Y. A. Elabd, *Macromolecules* **49:**3382-3394 (2016).

49 T. Seki, J.-D. Grunwaldt and A. Baiker, *J Phys Chem B* **113:**114-122 (2009).

50 M. C. Kroon, W. Buijs, C. J. Peters and G. J. Witkamp, *Thermochim Acta* **465:**40-47 (2007).

51 C. Maton, N. De Vos and C. V. Stevens, *Chem Soc Rev* **42:**5963-5977 (2013).

52 C. L. Beyler and M. M. Hirschler, *SFPE Handbook of Fire Protection Engineering* **2:**32 (2002).

53 E. Fitzer and D. J. Müller, *Carbon* **13:**63-69 (1975).

54 Y. Men, M. Siebenburger, X. Qiu, M. Antonietti and J. Yuan, *J Mater Chem A* **1:**11887-11893 (2013).

55 D. Salas-de la Cruz, M. D. Green, Y. S. Ye, Y. A. Elabd, T. E. Long and K. I. Winey, *J Polym Sci Part B: Polym Phys* **50:**338-346 (2012).

56 K. Artyushkova, B. Kiefer, B. Halevi, A. Knop-Gericke, R. Schlogl and P. Atanassov, *Chem Commun* **49:**2539-2541 (2013).

57 S. Brunauer, L. S. Deming, W. E. Deming and E. Teller, *J Am Chem Soc* **62:**1723-1732 (1940).